Carbohydrate Polymers 351 (2025) 123122

Contents lists available at ScienceDirect

Carbohydrate Polymers

journal homepage: www.elsevier.com/locate/carbpol

NMR spectroscopic studies of chitin oligomers – Resolution of individual residues and characterization of minor amide *cis* conformations

Piera Wiesinger, Gustav Nestor *

Department of Molecular Sciences, Swedish University of Agricultural Sciences, Almas Allé 5, Uppsala 75651, Sweden

ARTICLE INFO

Keywords:
Chitin oligomers
N-Acetylglucosamine
$(GlcNAc)_{2-6}$
NMR spectroscopy
$^{1}H,^{15}N$-HSQC
Amide proton
cis/trans isomerisation

ABSTRACT

Chitin is the second most abundant biopolymer in nature after cellulose and is composed of *N*-acetylglucosamine (GlcNAc) connected via β(1 → 4)-glycosidic bonds. Despite its prominence in nature and diverse roles in pharmaceutical and food technological applications, there is still a need to develop methods to study structure and function of chitin and its corresponding oligomers. Efforts have been made to analyse chitin oligomers by NMR spectroscopy, but spectral overlap has prevented any differentiation between the interior residues. In this study, chitin oligomers up to hexaose with natural abundance of ^{15}N were analysed with NMR spectroscopy in aqueous solution. Different $^{1}H,^{15}N$-HSQC pulse sequences were evaluated to obtain the best resolution and sensitivity. Interior residues were resolved in the ^{15}N dimension and detailed chemical shifts of amide proton and nitrogen are reported for the first time. Additionally, all oligomers were analysed for the presence of the amide *cis* form and its corresponding chemical shifts were assigned. This study exploits the information that can be obtained from chitin oligomers with NMR spectroscopy and depicts methods for detailed analysis of glycans containing oligomers of *N*-acetylglucosamine.

1. Introduction

Chitin, which is the second most abundant biopolymer after cellulose, is composed of *N*-acetylglucosamine (GlcNAc) units connected via β(1 → 4)-glycosidic linkages. The insoluble chitin polymer forms the solid shell of insects and crustaceans and is part of the cell wall of fungi, algae and yeasts (Moussian, 2019). Several industrial applications of chitin and its derivatives, such as chitosan, have been identified due to its biodegradability, stability, bioactivity and chelating and adsorbing ability. Chitosan is achieved by deacetylation to obtain higher water solubility and easier functionalization (Synowiecki & Al-Khateeb, 2003). Biodegradable, but strong and stable polymers are needed for pharmaceutical and agricultural applications (Ahmad et al., 2020; Kashyap et al., 2015). Food additives, food packaging material and pharmaceutical products benefit from its antimicrobial properties (Ahmad et al., 2020; Dutta et al., 2012). The chelation ability of chitin is utilized in environmental or food related applications, such as decontamination from heavy metals (Anastopoulos et al., 2017).

From a biological perspective, *N*-acetylglucosamine, its oligomers and homopolymer play a vital role in worldwide carbohydrate turnover due to its high abundance. Different enzymes are involved in the synthesis, degradation and recognition of chitin. Examples are chitin synthases, which are present in chitinous organisms (Merzendorfer, 2006; Pacheco-Arjona & Ramirez-Prado, 2014), and chitinases, which are chitin degrading enzymes found in archaea, bacteria and eukaryotes (Adrangi & Faramarzi, 2013; Itoh & Kimoto, 2019; Takashima et al., 2018) that help the organisms in defending themselves against pathogen or herbivore attacks (Fukamizo & Shinya, 2019). Another class of enzymes which catalyse the oxidative degradation of chitin and chitin oligomers is family 10, 11 and 15 of lytic polysaccharide monooxygenases (LPMOs) (Courtade & Aachmann, 2019). Some lectins, such as plant hevein, can recognize and bind to chitin oligomers (Colombo et al., 2005), which contributes to the plants' defense mechanisms (Peumans & Van Damme, 1995). For all of these proteins, no matter if being involved in synthesis, degradation or recognition of chitin, the mode and details of the interaction is crucial for the outcome.

Studies on structure-function relationships of chitin, chitosan and chitin oligomers require well-defined samples, where each residue is unambiguously identified as either GlcNAc or glucosamine (Tyrikos-Ergas et al., 2021). However, the analysis and structure determination of chitin and its corresponding oligomers in order to obtain a well-defined characterization of each GlcNAc residue is still a challenge. To

* Corresponding author.
E-mail addresses: piera.wiesinger@slu.se (P. Wiesinger), gustav.nestor@slu.se (G. Nestor).

https://doi.org/10.1016/j.carbpol.2024.123122
Received 19 September 2024; Received in revised form 3 December 2024; Accepted 4 December 2024
Available online 5 December 2024

determine the composition of complex glycans and substitution patterns, NMR spectroscopy is an invaluable tool, which can also give information about conformation and dynamics of glycans and their interactions with other biomolecules. However, a major challenge when studying chitin oligosacharides by NMR spectroscopy is spectral overlap of the individual residues due to almost identical electronic microenvironments in the repeating chain of GlcNAc. Only the reducing-end residue and to some degree the non-reducing-end residue can be identified by ^{1}H and ^{13}C NMR (Gagnaire et al., 1982; Germer et al., 2003; Li et al., 2019; Sugiyama et al., 2001). Resolution of overlapping signals from interior residues requires additional NMR spectroscopic solutions.

One approach for resolving individual residues is to utilize a mixture of water and DMSO, which could be used to partially differentiate the amide proton signals up to tetrasaccharide (Li et al., 2019). However, DMSO and other organic solvents may affect the conformation of glycans and proteins in studies on biological systems. A different approach utilizing subtle differences in ^{15}N chemical shifts has previously been applied on glycans containing amide groups (Blundell et al., 2004; Garádi et al., 2023; Langeslay et al., 2013; Pomin, 2013; Pomin et al., 2010). Taking advantage of the nitrogen dimension was shown to be helpful to separate individual residues and for facilitating identification of the glycans in mixtures. An early application of ^{15}N NMR experiments on ^{13}C/^{15}N-labelled hyaluronan oligosaccharides was reported by Blundell et al. (2004), where triple-resonance and ^{15}N-edited 3D experiments were applied to achieve resolution of GlcNAc amide resonances in hyaluronan oligosaccharides up to decamer. More recent examples are the characterization of differently sulphated GlcNAc and GalNAc in glycosaminoglycans (GAGs) (Pomin et al., 2010), of *N*-sulfoglucosamine in heparin and heparan sulfate (Langeslay et al., 2013) and of GlcNAc and Neu5Ac units in human milk oligosaccharides (Garádi et al., 2023; Garádi et al., 2025). The latter examples were performed on natural abundance ^{15}N, which is possible with the use of high concentrations and high-sensitive cryoprobes.

The strategy of using the ^{15}N dimension to resolve individual sugar residues has so far been limited to GAGs and milk oligosaccharides and has not been applied to chitin or its derivatives. In studies of chitin oligomers by 2D NMR experiments, only ^{1}H and ^{13}C resonances have been assigned, which limits the resolution of the individual residues to the trimer (Sugiyama et al., 2001). However, to this date it has not been shown how many GlcNAc residues directly next to each other that can be resolved with ^{15}N NMR spectroscopy.

An additional option that NMR spectroscopy provides is the analysis of minor conformations. In GlcNAc, the *cis* isomer of the *N*-acetyl group is present in ~1 % (Hu, Zhang, et al., 2010; Meredith et al., 2022; Xue & Nestor, 2022). We recently found that the amide proton of the GlcNAc *cis* form can be identified in ^{1}H NMR spectra, which allowed analysis of its conformation (Xue & Nestor, 2022). Yet, the appearance of amide *cis* forms in oligosaccharides containing GlcNAc, such as chitin oligomers, has not been described.

Here we addressed both the challenge of spectral overlap and detection of minor conformations when analysing chitin oligomers with NMR spectroscopy. We hypothesized that ^{15}N NMR would resolve interior residues of chitin oligomers and that minor amide *cis* forms would be present in chitin oligomers. Soluble chitin oligomers from dimer to hexamer were analysed in water at pH 6.5, in order to resemble biological conditions. Three different ^{1}H,^{15}N-HSQC pulse sequences were evaluated to obtain the best resolution and sensitivity for interior residues. Individual residues were resolved in the ^{15}N dimension, which enabled a detailed chemical shift assignment of chitinbiose to pentaose, including ^{1}H, ^{13}C and ^{15}N. The detection and assignment of the minor *cis* conformation was achieved by a combination of standard and band-selective 2D experiments. In addition, the *cis* form of chitin oligomers was quantified for the first time.

2. Experimental

2.1. Sample preparation

Isotopically unlabelled di-*N*-acetylchitobiose ($GlcNAc_2$, 60 mM final concentration), tri-*N*-acetylchitotriose ($GlcNAc_3$, 50 mM), penta-*N*-acetylchitopentaose ($GlcNAc_5$, 20 mM) and hexa-*N*-acetylchitohexaose ($GlcNAc_6$, 7 mM) were purchased from Megazyme (Bray, Ireland). The vendor claims a purity of >95 %. Tetra-*N*-acetylchitotetraose ($GlcNAc_4$, 40 mM) was purchased from Omicron Biochemicals (South Bend, IN, USA) (99.6 % purity). Each oligomer was dissolved in 90 % ultrapure distilled H_2O (Merck Millipore, MA, USA) and 10 % D_2O (Deutero GmbH, Kastellaun, Germany).The pH was adjusted to 6.5 with NaOH or HCl in H_2O:D_2O (9:1) by using a calibrated SpinTrode pH electrode (Hamilton, NV, USA). No additional buffer or salt components were used. The samples were transferred to 5 mm NMR tubes. The samples differed in their concentration, as it was always aimed for the highest soluble concentration. For internal referencing, non-deuterated sodium trimethylsilylpropanesulfonate (DSS) (Merck AG, Darmstadt, Germany) was added to a final concentration of 0.5 mM. All samples were kept at 4 °C for up to 12 months and data was collected during this period of time.

2.2. NMR spectroscopy experiments

All experiments for assignment purposes were performed at 25 °C with a Bruker Avance III 600 MHz spectrometer (Billerica, MA, USA) equipped with a 5 mm ^{1}H/^{13}C/^{15}N/^{31}P inverse detection CryoProbe. ^{1}H and ^{13}C chemical shifts were referenced to DSS (δ = 0.00 ppm). ^{15}N chemical shifts were indirectly referenced according to Wishart et al. (1995).

For processing of NMR spectra TopSpin 4.3.0 and for deconvolution and illustration purposes MestReNova software were used.

The 2D spectra were processed by using forward linear prediction on complex data in the indirect dimension F1. The data were zero-filled before applying a $\pi/2$ shifted sine-squared bell function in both dimensions, except for ^{1}H,^{15}N-HSQC-type spectra where a $\pi/3$ shifted function was used.

Three different ^{1}H,^{15}N-HSQC pulse sequences were compared: a fast-HSQC (FHSQC) (Mori et al., 1995), a band-selective excitation short-transient HSQC (BEST-HSQC) (Lescop et al., 2007; Schanda et al., 2006), and a cross-polarization assisted heteronuclear in-phase single-quantum correlation (CP-HISQC) experiment (Yuwen & Skrynnikov, 2014). Several parameters, including number of scans (32), number of increments (96) and the INEPT transfer delay (optimized for $^{1}J_{NH}$ = 92 Hz) were kept the same in all the three experiments to make them comparable. However, since BEST-HSQC is designed for very short acquisition times and relaxation delays, these parameters were set to 42 ms and 0.2 s, respectively, whereas the same parameters were set to 107 ms and 1.5 s, respectively, for the other experiments. More details are reported in Table S1. It should be pointed out that the cross-polarization element in the CP-HISQC experiment is potentially harmful for the probe if the duration or the power are increased excessively. In our case, using a modern cryoprobe, no sample heating was observed with 3.2 kHz ^{15}N *rf* field for 9 ms.

The following NMR experiments were used for resonance assignments: 1D-^{1}H, 1D-^{13}C, ^{1}H,^{15}N-HSQC, ^{1}H,^{15}N-HSQC-TOCSY, ^{1}H,^{13}C-HMBC, ^{1}H,^{13}C-HSQC, ^{1}H,^{13}C-HSQC-TOCSY and ^{1}H,^{1}H-NOESY. For the assignment of *cis* forms, the following spectra were used: 1D-^{1}H, 1D-^{13}C, ^{1}H,^{13}C-HSQC, ^{1}H,^{13}C-HSQC-TOCSY, ^{1}H,^{1}H-TOCSY, ^{1}H,^{1}H-NOESY and band-selective ^{1}H,^{1}H-TOCSY (Alexandersson et al., 2020). An overview of the experimental parameters is given in Table S1.

2.3. Quantification of cis forms with NMR spectroscopy

For the quantification of *cis* forms at different temperatures, a temperature calibration (Van Geet, 1968) was performed with a standard of 4 % methanol in methanol-d_4 (Bruker, MA, US) from 5 to 40 °C in 5 °C steps. With the same temperature series, ^{1}H NMR spectra were recorded for $(GlcNAc)_2$ and $(GlcNAc)_3$ with a relaxation delay of 10 s and 64 scans. After manual peak picking, a region of 2 ppm (δ = 8.6–6.6 ppm) was deconvoluted and fitted with a Lorentzian-Gaussian shape type in MestReNova. The population percentage of *cis* to *trans* form were calculated using the integrals of the NH signals. For each residue, the *trans/cis* equilibrium constant was calculated and thermodynamic parameters (ΔH°, ΔS° and ΔG°) were extracted from a van't Hoff plot.

3. Results and discussion

Chitin oligomers from disaccharide to hexasaccharide were used in this study, with numbering of the residues as shown in Table 1. All oligomers are named $(GlcNAc)_n$, where n is the number of residues. During the sample preparation the aim was to reach highest possible concentration for best results in sensitivity since the sugars were not isotopically labelled. The solubility of chitin oligomers decreases with increasing length; thus $(GlcNAc)_6$ at pH 6.5 only reached 7 mM, whereas $(GlcNAc)_2$ was easily dissolved as 60 mM in the same conditions. The amide protons of glucosaminoglycans are in pH dependent exchange with H_2O (Green et al., 2019). The pH 6.5 was chosen to resemble biological conditions and detect optimal line widths at the same time. Data from Green et al. (2019) suggest that NH resonance line widths of *N*-acetylated saccharides do not change at pH below 6.5, but increase at higher pH.

3.1. Evaluation of different ^{1}H,^{15}N-HSQC experiments

Different types of pulse sequences for ^{1}H,^{15}N-HSQC experiments are available and commonly used in protein NMR spectroscopy. However, they are seldom applied for carbohydrate analysis. Here we compared three pulse sequences to determine the best resolution and sensitivity of amide resonances with unlabelled chitin oligosaccharide samples (Fig. 1). All data presented here were recorded without non-uniform sampling (NUS). NUS is an invaluable sampling method in NMR spectroscopy to reduce the experiment time and/or increase the resolution of the indirect dimension. Here, 25 % NUS has been used for testing experiment setups and different evolution delays (data not shown). However, NUS artifacts and decreased sensitivity at 25 % NUS led to the conclusion that uniform sampling is more reliable for a detailed comparison. Nevertheless, we suggest testing NUS to reduce experiment times when applying the here presented experiments on similar samples.

A fast-HSQC (FHSQC) (Mori et al., 1995), a band-selective excitation short-transient HSQC (BEST-HSQC) (Lescop et al., 2007; Schanda et al., 2006) and a cross-polarization assisted heteronuclear in-phase single-quantum correlation (CP-HISQC) (Yuwen & Skrynnikov, 2014) spectrum were recorded on $(GlcNAc)_5$ with the same spectral width in the ^{15}N dimension. The spectra were compared in terms of resolution and sensitivity.

The FHSQC experiment was initially developed by Mori et al. (1995) for optimized sensitivity on exchanging protons. It includes a water flip-back WATERGATE-HSQC sequence that preserves water magnetization and enables magnetization transfer from water to labile protons. This approach enables relatively short recovery delays with preserved signal intensities. Similarly, the BEST-HSQC experiment allows fast acquisition based on the SOFAST pulse scheme, which was initially developed by Schanda et al. (2005) for experiments with instable proteins and for observation of fast dynamics. The BEST pulse sequence uses band-selective pulses to excite amide ^{1}H spins only, which leads to shorter T_1 relaxation times and thus enables faster recycling. Finally, the CP-HISQC developed by Yuwen and Skrynnikov (2014) for the study of disordered proteins, combines proton decoupling during the ^{15}N evolution delay t_1 (HISQC) with cross-polarization (CP) ^{1}H-^{15}N replacing the first INEPT transfer. The proton decoupling element removes effects of solvent exchange during t_1 by keeping the ^{15}N transverse coherence in-phase with respect to ^{1}H. Rapid water exchange leads to line broadening in the ^{15}N dimension of ^{1}H,^{15}N-HSQC spectra, but the proton decoupling during t_1 provides enhanced resolution, which was first identified by Bax et al. (1990) and later applied on lysine NH_3 groups by Iwahara et al. (2007). Additionally, the cross-polarization element included in the CP-HISQC improves the sensitivity of rapidly exchanging NH by magnetization transfer from water to amide protons and further to the amide nitrogens during the CP element (Yuwen & Skrynnikov, 2014).

When applying the three HSQC pulse sequences on chitin oligomers, the resulting spectra were markedly affected by different processing procedures. When applying forward linear prediction in the indirect dimension, which is a default option in Bruker software, the ^{15}N resolution improved for all three spectra, however artifacts appeared for the FHSQC spectrum (Fig. S1). Linear prediction is not recommended when signals are weak and approaching the noise level at the end of evolution time (Reynolds et al., 1997), which was the case for the FHSQC spectrum. All three spectra were compared with and without forward linear prediction and best results were obtained with the CP-HISQC pulse sequence (Table S2). The FHSQC experiment resulted in the worst sensitivity and resolution. The BEST-HSQC spectrum showed slightly better ^{15}N resolution than the FHSQC spectrum and the sensitivity (signal-to-noise ratio) was similar to or even better than the CP-HISQC spectrum. However, the BEST-HSQC showed considerable differences in signal-to-noise between different cross-peaks, which may be attributed to the much faster repetition rate used for the BEST-HSQC experiment, making the intensities more sensitive to differences in relaxation times of the amide protons.

Table 1
Overview of chitin oligomers and the corresponding nomenclature used in this study. All oligomers were isotopically unlabelled. The non-reducing end residue is ω; the reducing end residue is α or β; the residue adjacent to the reducing end residue is γ^α or γ^β depending on the anomeric configuration of the reducing end; internal residues are named ζ, ε and δ accordingly.

Sample	Numbering of residues	n internal residues	Scheme
$(GlcNAc)_2$	ω, α/β	0	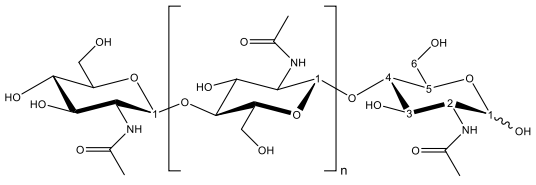
$(GlcNAc)_3$	ω, $\gamma^{\alpha/\beta}$, α/β	1	
$(GlcNAc)_4$	ω, δ, $\gamma^{\alpha/\beta}$, α/β	2	
$(GlcNAc)_5$	ω, ε, δ, $\gamma^{\alpha/\beta}$, α/β	3	
$(GlcNAc)_6$	ω, ζ, ε, δ, $\gamma^{\alpha/\beta}$, α/β	4	

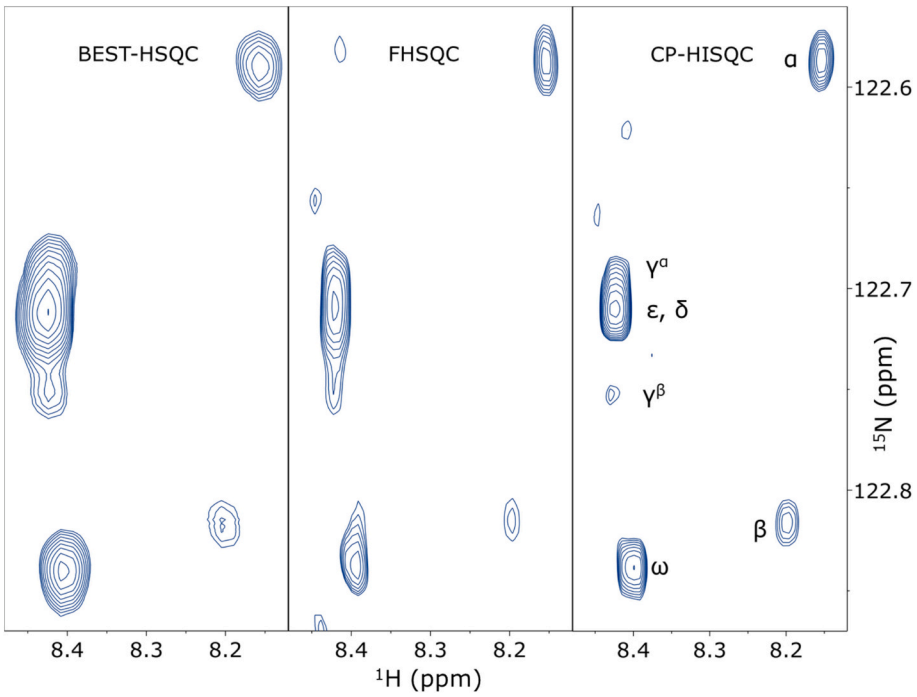

Fig. 1. Comparison of $^{1}H,^{15}N$-HSQC spectra of $(GlcNAc)_5$ with corresponding residue assignments of amide *trans* signals. Three different pulse sequences were used, (from left to right) namely BEST-HSQC, FHSQC and CP-HISQC. No linear prediction was applied during processing. Comparison of signal-to-noise ratios and line half widths are shown in Table S2. NHα crosspeaks are folded in the spectra.

Given the short experimental time for the BEST-HSQC experiment, this experiment is a good alternative when sensitivity is the most important factor. However, since CP-HISQC experiments provided both the best resolution and excellent sensitivity, this pulse sequence was selected for further analysis of chitin oligosaccharides of different length.

3.2. *Resolving spectral overlap in the ^{15}N dimension*

The amide proton signals of *N*-acetylglucosamine and chitin disaccharide are resolved in 1D ^{1}H spectra, but oligomers larger than disaccharide show spectral overlap of NH signals as pointed out in Fig. 2. With this overlap, information about individual residues is limited.

To explore the limits of spectral resolution of NH signals in the

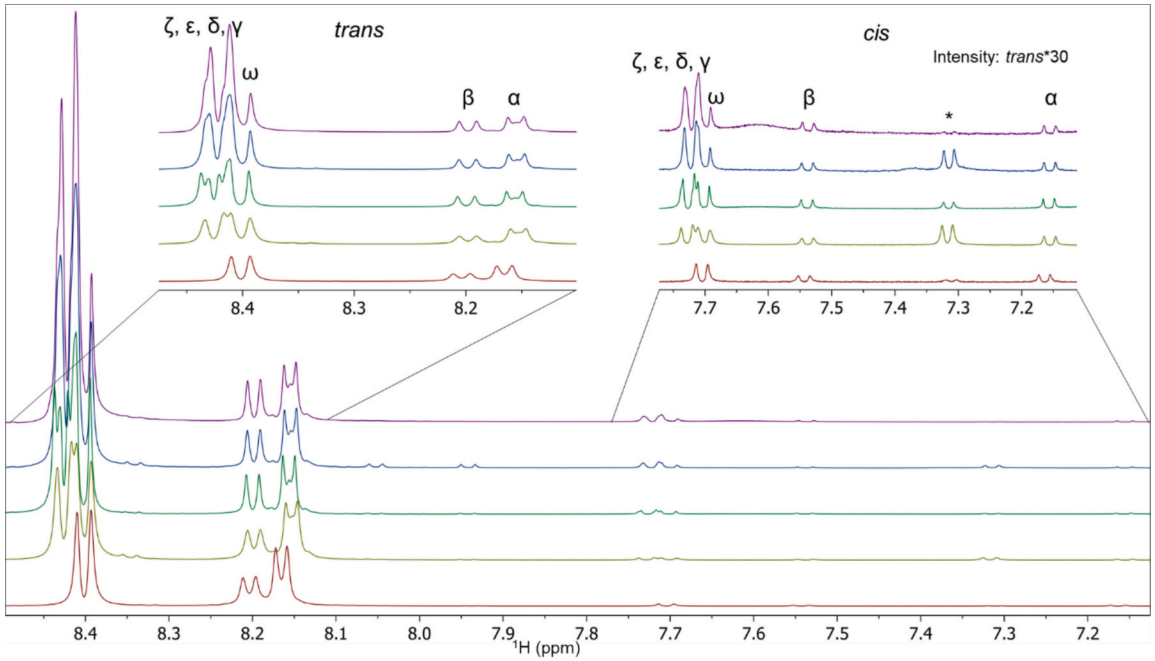

Fig. 2. 1D ^{1}H spectra of (from bottom to top) $(GlcNAc)_2$, $(GlcNAc)_3$, $(GlcNAc)_4$, $(GlcNAc)_5$ and $(GlcNAc)_6$ with corresponding residue assignments of amide *trans* (top left inset) and *cis* (top right inset, amplified 30 times) signals. The spectra are normalized to the α_{trans} signal. The numbering of residues is described in Table 1. The asterisk (*) denotes an unknown impurity. Herein we show that the spectral overlap of amide proton signals in the ^{1}H dimension is present from degree of polymerisation 3 (DP3) and higher and information about individual residues is limited.

nitrogen dimension, $^{1}H,^{15}N$-HSQC experiments were recorded on chitin oligosaccharides from dimer to hexamer. The ^{15}N resolution is limited by relaxation during the evolution delay (t_1) and t_1 >0.8 s did not improve resolution, but sensitivity was significantly reduced. A narrow ^{15}N spectral width of only 1.0 ppm (equivalent to t_1 = 0.79 s with 96 increments) results in folding of the NH signal of the reducing end in α configuration. In Fig. 3 the NH regions of $^{1}H,^{15}N$-HSQC spectra of each oligomer are overlaid, which shows well resolved NH signals from the α, β, ω and γ^{α} or γ^{β} residues in all studied oligomers. Spectral resolution of the δ interior residue of the tetramer is also achieved. When increasing the degree of polymerisation (DP) to 5 the interior residues δ and ε are overlapping, but the interior γ^{α} or γ^{β} are still resolved. For $(GlcNAc)_6$ γ^{α}, δ, ε and ζ are overlapping, but γ^{β} is clearly separated. The $^{1}H,^{15}N$-HSQC spectra can thus resolve all the residues up to $(GlcNAc)_4$ and for $(GlcNAc)_5$ and $(GlcNAc)_6$ the interior residues (δ, ε and ζ) start to overlap also in the ^{15}N dimension. Compared to 1D 1H spectra, where only α and β residues are completely resolved for oligomers larger than disaccharide, this is a substantial improvement.

The separation of NH signals of individual residues through the nitrogen dimension allows to extend the gained resolution to the ring protons of each spin system by applying $^{1}H,^{15}N$-HSQC-TOCSY experiments (Fig. 4). By this means, also ring protons that are completely unresolved in the respective oligomers can be traced to the individual residues. It is to be noted that the pulse sequence of this $^{1}H,^{15}N$-HSQC-TOCSY is similar to the FHSQC experiment and both show a lower sensitivity for βNH compared to the CP-HISQC. This could be due to differences in relaxation or exchange rates, but was not investigated further within this study. Before using the 2D spectra for quantitative analysis, this discrepancy would need to be analysed.

3.3. Chemical shift assignment of $(GlcNAc)_{2–6}$

For chemical shift assignments of $(GlcNAc)_{2–6}$ a number of 2D NMR experiments were performed, including $^{1}H,^{13}C$-HSQC, $^{1}H,^{15}N$-HSQC, $^{1}H,^{13}C$-HMBC, $^{1}H,^{13}C$-HSQC-TOCSY and $^{1}H,^{15}N$-HSQC-TOCSY. The assignments (Tables S3 and S4) are in alignment with previous literature data (Gagnaire et al., 1982; Germer et al., 2003; Li et al., 2019; Sugiyama et al., 2001; Tokuyasu et al., 1997). For the first time, we can also report a detailed assignment of ^{15}N and $^{1}H(N)$ chemical shifts for $(GlcNAc)_{2–6}$ (Table 2), which was possible after resolving the crosspeaks in $^{1}H,^{15}N$-HSQC spectra. In contrast to the assignment of Li et al. (2019) of $(GlcNAc)_4$ in 70 % H_2O: 30 % DMSO-d_6 solvent, the here presented assignment of amide protons and nitrogens is in H_2O pH 6.5 and detailed up to the limit of resolution. Additionally, by recording $^{1}H,^{15}N$-HSQC-TOCSY experiments detailed ^{1}H chemical shifts of interior residues (γ^{α}, γ^{β} and δ) for trimer and tetramer could be determined (Table S3).

3.4. Chemical shift assignment of cis forms of $(GlcNAc)_{2–4}$

The amide *trans* and *cis* conformation of *N*-acetylglucosamine are shown in Scheme 1. Rotation around the NH-C(O) bond (θ_2) leads to two different conformations of the *N*-acetyl group, where the *trans* conformation is the most populated (~99 %) (Xue & Nestor, 2022). In this study, we observed the amide *cis* conformation despite its low abundance throughout all residues of chitin oligomers, which was detected from NH protons in 1D ^{1}H experiments. The exchange between *trans* and *cis* conformation was detected for $(GlcNAc)_{2–4}$ by 2D EXSY (Fig. 5 and Fig. S2) and selective 1D EXSY (Fig. S3) experiments. For the assignment of signals from the *cis* form of $(GlcNAc)_{2–4}$, 1D ^{1}H and 2D $^{1}H,^{13}C$-HSQC,

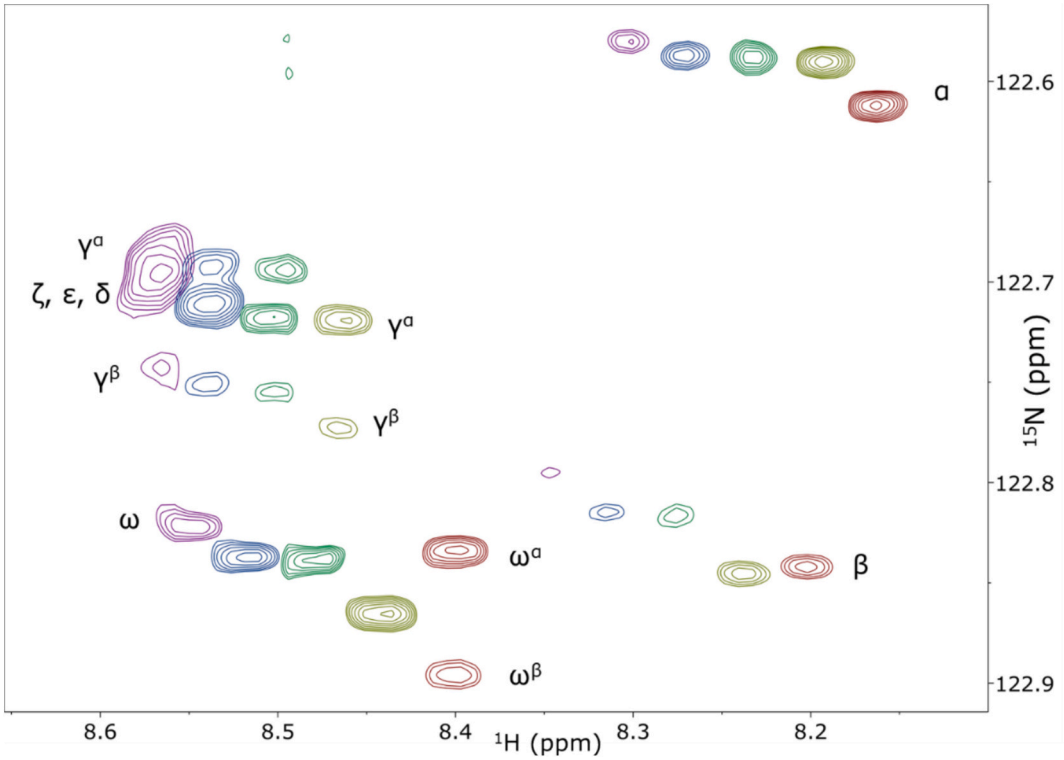

Fig. 3. $^{1}H,^{15}N$-CP-HISQC spectra of (from right to left) $(GlcNAc)_2$, $(GlcNAc)_3$, $(GlcNAc)_4$, $(GlcNAc)_5$ and $(GlcNAc)_6$ with corresponding residue assignments of signals. For illustration purposes the spectra of $(GlcNAc)_{3–6}$ are shifted downfield in the ^{1}H dimension. NHα crosspeaks are folded in the spectrum. The numbering of residues is described in Table 1. Herein we show that the spectral overlap of amide proton signals in the ^{1}H dimension is resolved in the ^{15}N dimension to a large extent with a spectral width of 1 ppm.

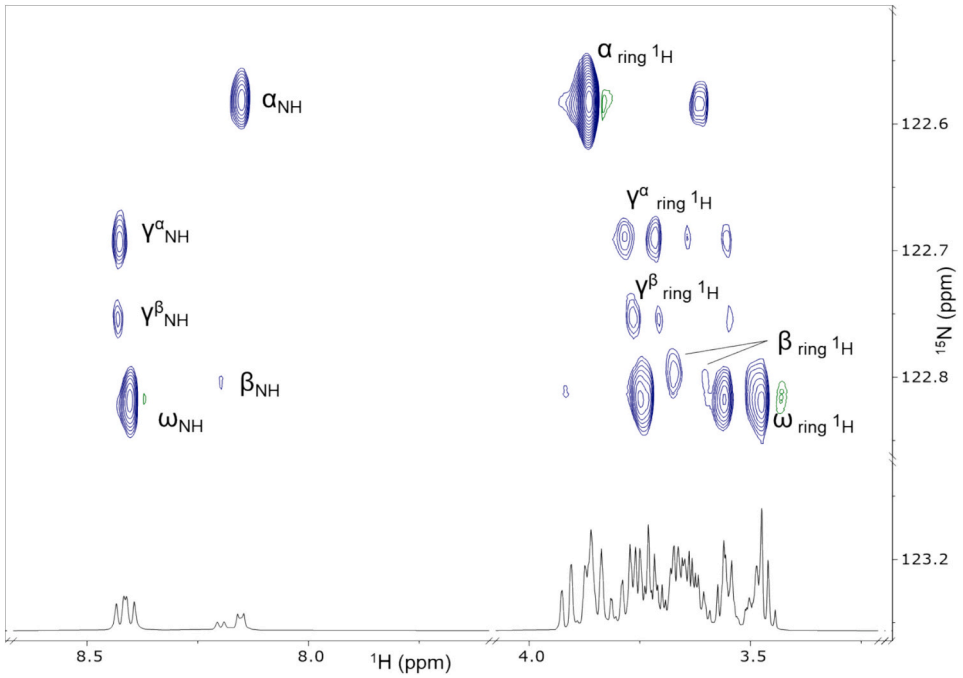

Fig. 4. $^{1}H,^{15}N$-HSQC-TOCSY spectrum of $(GlcNAc)_3$ (100 ms mixing time; without linear prediction in f1) showing amide proton and ring proton regions (except for H1). Assignments of signals within individual residues are highlighted (full assignment in Table S3). The α crosspeaks are folded in the spectrum. The numbering of residues is described in Table 1. Herein we show that overlapping ring protons of different residues/spin systems are resolved in the ^{15}N dimension.

Table 2
Chemical shift assignment of amide ^{15}N and ^{1}H of $(GlcNAc)_{2-6}$ (ppm).

		N	HN
$(GlcNAc)_2$	α	123.61	8.16
	β	122.84	8.20
	ω (α, β)	122.83, 122.90	8.40
$(GlcNAc)_3$	α	123.59	8.15
	β	122.85	8.20
	γ (α, β)	122.77, 122.72	8.42
	ω	122.86	8.40
$(GlcNAc)_4$	α	123.59	8.15
	β	122.82	8.20
	γ (α, β)	122.70, 122.76	8.41, 8.42
	δ	122.72	8.43
	ω	122.84	8.40
$(GlcNAc)_5$	α	123.59	8.15
	β	122.81	8.20
	γ (α, β)	122.69, 122.75	8.42
	δ, ε	122.71	8.42
	ω	122.84	8.40
$(GlcNAc)_6$	α	123.58	8.15
	β	122.79	8.20
	γ (α, β)	122.68, 122.74	8.42
	δ, ε, ζ	122.68–122.71	8.42
	ω	122.82	8.40

band-selective (Fig. S4) and non-selective TOCSY experiments were used. Resonances from H1-H3, (N)H, C1 and C2 could be assigned (Table 3), which are the ^{1}H and ^{13}C resonances that are assumed to be most divergent between *trans* and *cis* forms. Differences in chemical shift compared to the *trans* form were calculated and the results show that H2, NH and C2 chemical shifts are most affected by the exchange (Table 3). The assignments are in alignment with data from the monomeric GlcNAc (Xue & Nestor, 2022). However, *cis* NH could not be detected in $^{1}H,^{15}N$-HSQC spectra because the samples were isotopically unlabelled and the *cis* form occurs in low percentages, and thus *cis* form ^{15}N resonances could not be assigned.

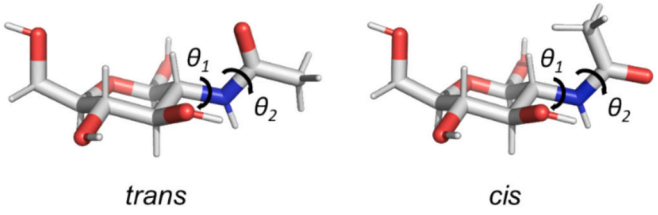

Scheme 1. *Trans* and *cis* conformation of the amide group of β-GlcNAc due to rotation around torsion angle θ_2 (C2-N-CO-CH_3) (blue: nitrogen, red: oxygen). The torsion angle θ_1 (H2-C2-N-NH) is assumed to be in *syn* ($\theta_1 = 0°$) or *anti* ($\theta_1 = 180°$) conformation (here shown in *anti*) and relates to $^{3}J_{\underline{NH},H2}$ coupling constants.

3.5. Quantification of the amide cis form

To quantify the population of *cis* and *trans* conformations, quantitative 1D-^{1}H experiments with long recovery delay (10 s) in a temperature range of 3–42 °C were performed with $(GlcNAc)_2$ and $(GlcNAc)_3$. Due to spectral overlap of interior and the non-reducing end residues longer chitin oligomers were not used for quantification. The *trans* and *cis* populations (Fig. S5) were obtained by integration of the NH signals and were used to calculate equilibrium constants (Table S5) and thermodynamic parameters (Table 4). The exchange of the amide protons with water might affect the integrals. However, we expect the exchange rate of the different configurations and conformations to be similar and thus the exchange should have a negligible effect on the relative quantification.

The *cis* conformation was present with 1.8 % in the non-reducing end residue (ω) and 1.0–1.1 % in the reducing end residue (α + β) at 25 °C in both oligomers and with 1.6 % in the interior residue (γ) of $(GlcNAc)_3$. The *cis* form population increased for all residues with increasing temperature. An increase from 1.1 to 1.3 % to 2.2–2.4 % for ω and γ and 0.6 % to 1.6 % for α + β was observed between 3 and 42 °C. Previously, an increase from 0.9 to 2.2 % for α + β has been described for the monomer *N*-acetylglucosamine when elevating the temperature from 3 to 40 °C

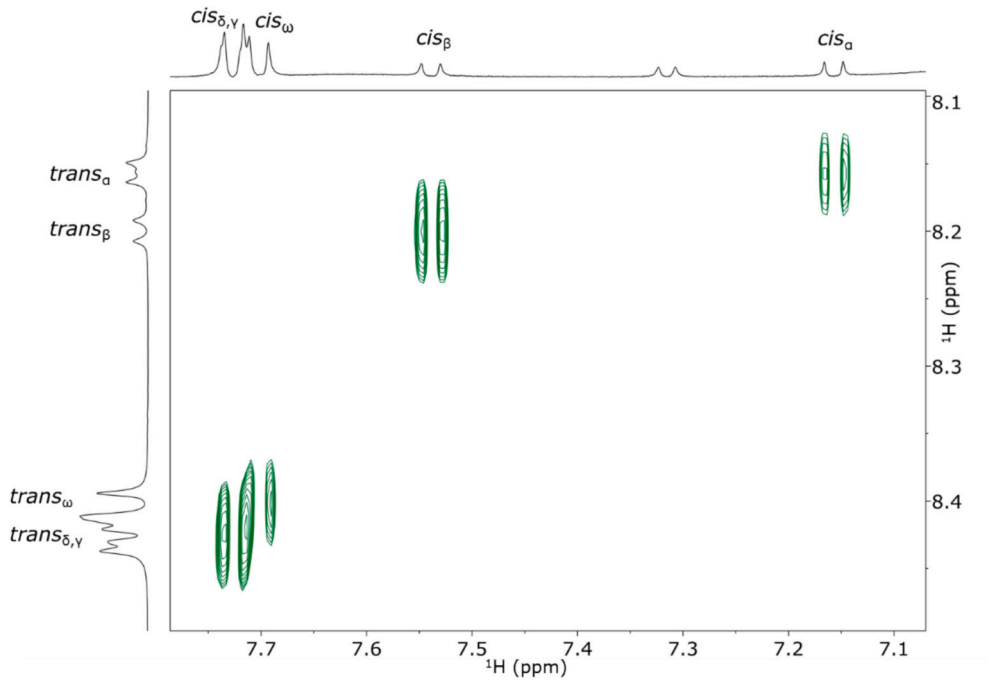

Fig. 5. Selected region of a 2D EXSY spectrum (τ_{mix} = 400 ms) of $(GlcNAc)_4$ showing the NH *trans/cis* exchange. Corresponding assignments of protons from ω, δ, γ, α and β residues are highlighted (assignment Table 2 and Table 3).

Table 3
^{1}H and ^{13}C chemical shift assignment of $(GlcNAc)_{2-4}$ amide *cis* forms (ppm); chemical shift differences compared to the amide *trans* form (Table S3 and S4) were calculated and the ranges of difference are presented here as $\Delta_{cis\text{-}trans}$ (ppm).

		H1	H2	H3	HN	C1	C2
$(GlcNAc)_2$	α	5.25	3.61	3.85	7.16	93.7	60.2
	β	4.70	3.32	3.67	7.54	n.d.[1]	63.4
	ω $^{(\alpha/\beta)}$	4.56	3.43	3.56	7.70	104.0	62.6
$(GlcNAc)_3$	α	5.23	3.61	3.86	7.15	n.d.	n.d.
	β	4.68	3.32	3.65	7.54	n.d.	n.d.
	γ $^{(\alpha/\beta)}$	4.55	3.45	3.68	7.73	n.d.	n.d.
	ω	4.55	3.43	3.50	7.70	n.d.	62.6
$(GlcNAc)_4$	α	5.23	3.60	3.86	7.15	n.d.	60.2
	β	4.70	3.31	3.64	7.54	n.d.	63.4
	γ $^{(\alpha/\beta)}$	4.55	3.46	3.67	7.73	103.8	62.0
	δ	4.55	3.46	3.67	7.73	103.8	62.0
	ω	4.55	3.42	3.54	7.70	104.1	62.6
$\Delta_{cis\text{-}trans}$		+0.06 to −0.05	−0.25 to −0.37	+0 to −0.07	−0.66 to −1.01	+0.58 to −0.08	+4.56 to +3.82

[1] n.d. = not determined.

Table 4
Thermodynamic parameters of the *cis→trans* isomerisation of $(GlcNAc)_2$ and $(GlcNAc)_3$ including enthalpy ΔH°, entropy ΔS° and Gibbs free energy ΔG°; calculated standard errors are shown with ±.

		α	β	γ	ω
$(GlcNAc)_2$	ΔH° (kJ/mol)	−16 ± 3	−16 ± 4	–	−15 ± 2
	ΔS° (J/K/mol)	−15 ± 10	−22 ± 13	–	−18 ± 7
	ΔG° (kJ/mol)	−12 ± 4	−10 ± 5	–	−10 ± 3
$(GlcNAc)_3$	ΔH° (kJ/mol)	−20 ± 2	−17 ± 4	−14 ± 2	−15 ± 2
	ΔS° (J/K/mol)	−28 ± 6	−23 ± 13	−15 ± 6	−18 ± 5
	ΔG° (kJ/mol)	−12 ± 3	−10 ± 5	−10 ± 3	−10 ± 2

(Xue & Nestor, 2022). Correspondingly to the observations from the monomer, the β-*cis* form of the dimer and trimer are slightly more populated than the α-*cis* form (data not shown), which is the opposite relation compared to the α- and β-*trans* forms.

From the quantified conformations, the equilibrium constants $K_{(trans/cis)}$ (Table S5) were calculated, van't Hoff plots (Fig. 6) were built and thermodynamic parameters at 25 °C, including enthalpy $\Delta H^\circ_{cis\rightarrow trans}$, entropy $\Delta S^\circ_{cis\rightarrow trans}$ and Gibbs free energy $\Delta G^\circ_{cis\rightarrow trans}$, were calculated. The parameters show that the *cis* form is enthalpically and thermodynamically disfavoured, but entropically favoured throughout all residues. Both for $(GlcNAc)_2$ and $(GlcNAc)_3$ $\Delta G^\circ_{cis\rightarrow trans}$ is most negative for α (−12 kJ/mol), which was also shown previously for GlcNAc (Xue & Nestor, 2022). All other residues show similar values for $\Delta G^\circ_{cis\rightarrow trans}$ (−10 kJ/mol).

In summary, the reducing end α and β *cis* forms are less populated than the *cis* forms of the interior and non-reducing end residues. This is consistent with the observation that the α-*cis* form is thermodynamically least favoured. Given that the amount of amide *cis* form in the interior residue (γ) of chitin triose is similar to the β and ω *cis* forms and that *cis* forms from interior residues of chitin oligosaccharides up to hexamer could be observed, it is likely that amide *cis* forms are present also in larger oligomers and polymers of chitin. Whether the amide *cis* form plays any role in chitin conformation or in chitin specificity of chitinases and chitin-binding proteins is still an open question. It also remains to be investigated to what extent pH and salt concentration have an effect on the amount of the amide *cis* form, in order to draw conclusions about physiological conditions.

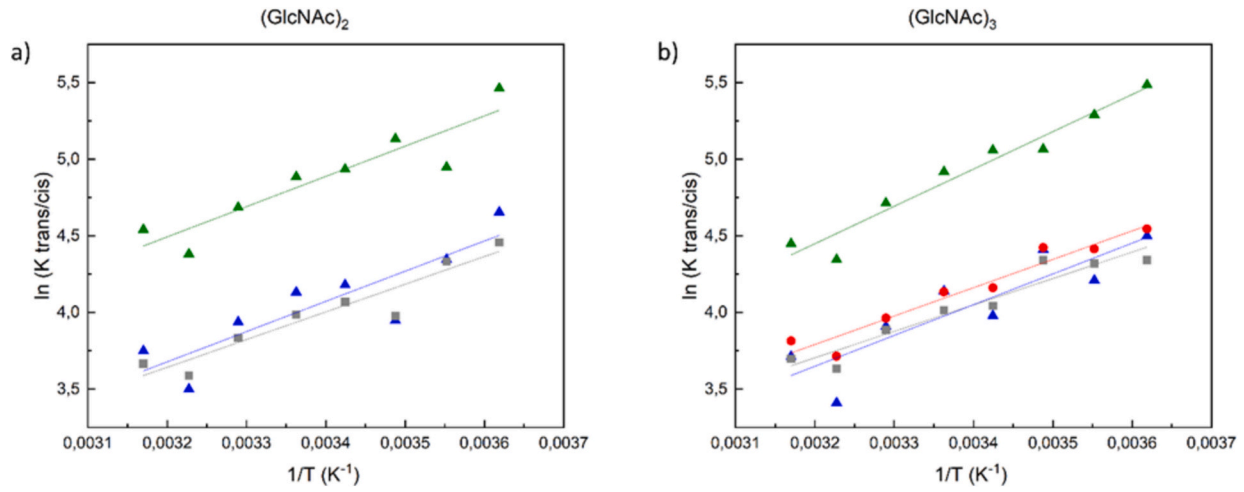

Fig. 6. Van't Hoff plots of the equilibrium between *trans* and *cis* amide forms from α (green Δ), β (blue Δ), γ (red ○) and ω (grey □) residues of (a) $(GlcNAc)_2$ and (b) $(GlcNAc)_3$.

Table 5
$^3J_{N\underline{H},H2}$ (Hz) and temperature coefficients dδ/dT (ppb/°C) of amide protons in chitin oligosaccharides and GlcNAc.

		trans		*cis*	
		$^3J_{N\underline{H},H2}$[1]	dδ/dT	$^3J_{N\underline{H},H2}$[1]	dδ/dT
GlcNAc[2]	α	8.8 ± 0.02	−9.1	10.6 ± 0.18	−6.9
	β	9.5 ± 0.01	−7.9	10.2 ± 0.26	−8.5
$(GlcNAc)_2$	α	8.2 ± 0.04	−8.5	10.9 ± 0.15	−6.5
	β	9.1 ± 0.03	−7.1	11.1 ± 0.13	−7.7
	ω (α/β)	10.1 ± 0.05	−7.4	11.0 ± 0.16	−7.6
$(GlcNAc)_3$	α	8.5 ± 0.26	−8.1	10.6 ± 0.36	−6.2
	β	9.2 ± 0.08	−6.9	11.1 ± 0.13	−7.3
	γ (α/β)	10.0 ± 0.28	−7.5	11.0 ± 0.10	−7.3
	ω	10.3 ± 0.23	−7.3	11.4 ± 0.30	−7.3
$(GlcNAc)_4$	α	8.7 ± 0.02		10.9 ± 0.15	
	β	9.2 ± 0.03		11.1 ± 0.18	
	γ (α/β)	9.5 ± 0.25		11.0 ± 0.26	
	δ	9.5 ± 0.25		10.7 ± 0.26	
	ω	10.1 ± 0.19		11.1 ± 0.29	
$(GlcNAc)_5$, $(GlcNAc)_6$ (only *trans*)	α	8.7 ± 0.02		10.8 ± 0.04	
	β	9.3 ± 0.03		11.0 ± 0.02	
	γ (α/β)	9.4 ± 0.11		10.8 ± 0.13	
	δ, ε, (ζ)	9.4 ± 0.11		10.8 ± 0.13	
	ω	9.9 ± 0.13		10.8± 0.18	

[1] A set of five 1D ^{1}H spectra for each compound and deconvolution were used to determine $^3J_{N\underline{H},H2}$ and the corresponding standard deviation.
[2] Data from Xue and Nestor (2022).

3.6. $^3J_{N\underline{H},H2}$ coupling constants and NH temperature coefficients

In order to gain conformational information about the *N*-acetyl group, $^3J_{N\underline{H},H2}$ coupling constants were measured from 1D ^{1}H spectra of all studied chitin oligomers, as far as spectral overlap in 1D ^{1}H spectra allowed (Table 5). $^3J_{N\underline{H},H2}$ coupling constants relate to the H2-C2-N-NH torsion angle (θ_1), which is assumed to be in *syn* ($\theta_1 = 0°$) or *anti* ($\theta_1 = 180°$) conformation (Scheme 1). For the reducing-end residue of chitin oligomers, $^3J_{N\underline{H},H2}$ was determined to be 8.2–8.7 Hz and 9.1–9.3 Hz for α_{trans} and β_{trans}, respectively, which is comparable to values measured for the GlcNAc monomer with 8.8 and 9.5 Hz for α_{trans} and β_{trans}, respectively (Xue & Nestor, 2022). The interior and non-reducing end residues showed slightly higher $^3J_{N\underline{H},H2}$ of the amide *trans* forms, with 9.4–10.0 Hz for γ and δ and 9.9–10.3 Hz for ω. Similarly, $^3J_{N\underline{H},H2}$ of the amide *cis* form, which were all in the range 10.6–11.4 Hz, were close to the GlcNAc monomer with α_{cis} 10.6 and β_{cis} 10.2 Hz.

The θ_1 torsion angle in the GlcNAc monosaccharide is predominantly in the *anti* conformation, which has been extensively investigated by measuring up to six *J*-couplings that are sensitive to θ_1 (Hu, Carmichael, et al., 2010; Meredith et al., 2022; Xue & Nestor, 2022). $^3J_{N\underline{H},H2}$ is not enough to provide definite conclusions about the conformation, because the difference between *anti* and *syn* conformation is small (1–2 Hz). Additionally, the calculated $^3J_{N\underline{H},H2}$ from parametrized Karplus equations are in general higher in magnitude (1–2 Hz) compared to experimental data of GlcNAc, which has been explained by internal dynamics of the pyranose ring (Mobli & Almond, 2007). The slightly higher $^3J_{N\underline{H},H2}$ of the amide forms of interior and non-reducing end residues could thus be due to less dynamic rings, but with the same *anti* conformation. The amide *cis* form is known to have larger $^3J_{N\underline{H},H2}$ than the *trans* form of about 2 Hz, which is shown also from the present data. To draw more conclusion about the θ_1 conformation of the *N*-acetyl group, more coupling constants sensitive to the torsion angle would be needed. Such an extensive investigation was recently performed on methyl β-chitobioside, showing exclusively *anti* conformations for both residues (Meredith et al., 2022).

Temperature coefficients dδ/dT (ppb/°C) of exchangeable protons (Table 5) can be indicative for inter- and intramolecular interactions, such as hydrogen bonds or steric effects and solvent accessibility (Blundell & Almond, 2007; Cierpicki & Otlewski, 2001). We determined temperature coefficients for chitinbiose and chitintriose over the

temperature range 3–42 °C. The chemical shifts were linear with temperature ($R^2 > 0.99$) which indicates that no big structural changes occur over the temperature range in solution (Blundell & Almond, 2007). All coefficients were between −6.2 and − 8.5 ppb/°C, with $(GlcNAc)_3$ showing slightly less negative values compared to $(GlcNAc)_2$. Generally, temperature coefficients of −10 to −6 ppb/°C indicate a lack of inter- and intramolecular hydrogen bonds (Baxter & Williamson, 1997; Dyson et al., 1988). The most notable difference between *trans* and *cis* conformation is that of the reducing end in α configuration. Here the amide *cis* form showed 2 ppb/°C less negative values compared to the *trans* form. A change of dδ/dT of α_{cis} compared to α_{trans} towards less negative values was also observed for monomeric *N*-acetylglucosamine and could indicate a decrease in solvation of the *cis* form due to steric effects or transient intra- or intermolecular hydrogen bonds (Xue & Nestor, 2022).

4. Conclusions

One of the biggest challenges of NMR analysis of carbohydrates is spectral overlap, which is especially severe for repeating residues that are identical, such as oligomers of chitin and cellulose. Studies on structure-function relationships of chitin and chitosan oligomers require detailed knowledge about individual residues. Here, we have shown that individual residues of chitin oligomers can be resolved by $^{1}H,^{15}N$-HSQC experiments using a narrow ^{15}N spectral width. A complete assignment of amide ^{15}N and ^{1}H was obtained and even residue-specific information about ring protons could be gained when applying a combination of $^{1}H,^{15}N$-HSQC and $^{1}H,^{15}N$-HSQC-TOCSY experiments. Three different $^{1}H,^{15}N$-HSQC type experiments were compared, showing that the CP-HISQC experiment resulted in the best resolution and consistent excellent sensitivity across all resonances.

Next to the approach for resolving individual residues, we also present a detailed analysis of the minor amide *cis* conformation in chitin oligomers. The amide *cis* form was detected from ^{1}H NMR spectra of all oligomers from dimer to hexamer. A limiting factor for the detection and analysis is the low natural abundance of the NMR active ^{15}N isotope. Despite this challenge of low sensitivity, ^{1}H and ^{13}C chemical shifts of the *cis* form could be assigned up to the tetramer by using band-selective NMR experiments. The amide *cis* forms of $(GlcNAc)_2$ and $(GlcNAc)_3$ were quantified to 1.0–1.8 % throughout all residues at 25 °C and thermodynamic parameters were calculated. Up to date it is not known to which extent the *cis* form plays a role in a biological context. The here presented data can contribute to facilitate the detection and quantitative analysis of the amide *cis* form in NMR studies on chitin and other glycans and glycoconjugates containing GlcNAc.

CRediT authorship contribution statement

Piera Wiesinger: Writing – original draft, Visualization, Methodology, Investigation, Formal analysis, Data curation. **Gustav Nestor:** Writing – review & editing, Validation, Supervision, Resources, Project administration, Methodology, Investigation, Funding acquisition, Conceptualization.

Declaration of competing interest

The authors declare that they have no known competing financial interests or personal relationships that could have appeared to influence the work reported in this paper.

Acknowledgements

This work was supported by the Swedish Research Council for Sustainable Development (Formas) [grant number 2021-01784] and the Royal Swedish Academy of Agriculture and Forestry [grant number 2022-0027].

Appendix A. Supplementary data

Supplementary data to this article can be found online at https://doi.org/10.1016/j.carbpol.2024.123122.

Data availability

Data will be made available on request.

References

Adrangi, S., & Faramarzi, M. A. (2013). From bacteria to human: A journey into the world of chitinases. *Biotechnology Advances, 31*(8), 1786–1795. https://doi.org/10.1016/j.biotechadv.2013.09.012

Ahmad, S. I., Ahmad, R., Khan, M. S., Kant, R., Shahid, S., Gautam, L., … Hassan, M. I. (2020). Chitin and its derivatives: Structural properties and biomedical applications. *International Journal of Biological Macromolecules, 164*, 526–539. https://doi.org/10.1016/j.ijbiomac.2020.07.098

Alexandersson, E., Sandström, C., Lundqvist, L. C. E., & Nestor, G. (2020). Band-selective NMR experiments for suppression of unwanted signals in complex mixtures. *RSC Advances, 10*(54), 32511–32515. https://doi.org/10.1039/D0RA06828D

Anastopoulos, I., Bhatnagar, A., Bikiaris, D. N., & Kyzas, G. Z. (2017). Chitin adsorbents for toxic metals: A review. *International Journal of Molecular Sciences, 18*(1), 114. https://www.ncbi.nlm.nih.gov/pmc/articles/PMC5297748/pdf/ijms-18-00114.pdf.

Bax, A., Ikura, M., Kay, L. E., Torchia, D. A., & Tschudin, R. (1990). Comparison of different modes of two-dimensional reverse-correlation NMR for the study of proteins. *Journal of Magnetic Resonance (1969), 86*(2), 304–318. https://doi.org/10.1016/0022-2364(90)90262-8

Baxter, N. J., & Williamson, M. P. (1997). Temperature dependence of 1H chemical shifts in proteins. *Journal of Biomolecular NMR, 9*(4), 359–369. https://doi.org/10.1023/A:1018334207887

Blundell, C. D., & Almond, A. (2007). Temperature dependencies of amide 1H- and 15N-chemical shifts in hyaluronan oligosaccharides. *Magnetic Resonance in Chemistry, 45*(5), 430–433. https://doi.org/10.1002/mrc.1969

Blundell, C. D., DeAngelis, P. L., Day, A. J., & Almond, A. (2004). Use of 15N-NMR to resolve molecular details in isotopically-enriched carbohydrates: Sequence-specific observations in hyaluronan oligomers up to decasaccharides. *Glycobiology, 14*(11), 999–1009. https://doi.org/10.1093/glycob/cwh117

Cierpicki, T., & Otlewski, J. (2001). Amide proton temperature coefficients as hydrogen bond indicators in proteins. *Journal of Biomolecular NMR, 21*(3), 249–261. https://doi.org/10.1023/A:1012911329730

Colombo, G., Meli, M., Canada, J., Asensio, J. L., & Jimenez-Barbero, J. (2005). A dynamic perspective on the molecular recognition of chitooligosaccharide ligands by hevein domains. *Carbohydrate Research, 340*(5), 1039–1049. https://doi.org/10.1016/j.carres.2005.01.044

Courtade, G., & Aachmann, F. L. (2019). Chitin-active lytic polysaccharide monooxygenases. In Q. Yang, & T. Fukamizo (Eds.), *Targeting chitin-containing organisms* (pp. 115–129). Springer Singapore. https://doi.org/10.1007/978-981-13-7318-3_6.

Dutta, J., Tripathi, S., & Dutta, P. K. (2012). Progress in antimicrobial activities of chitin, chitosan and its oligosaccharides: A systematic study needs for food applications. *Food Science and Technology International, 18*(1), 3–34. https://doi.org/10.1177/1082013211399195

Dyson, H. J., Rance, M., Houghten, R. A., Lerner, R. A., & Wright, P. E. (1988). Folding of immunogenic peptide fragments of proteins in water solution: I. Sequence requirements for the formation of a reverse turn. *Journal of Molecular Biology, 201*(1), 161–200. https://doi.org/10.1016/0022-2836(88)90446-9

Fukamizo, T., & Shinya, S. (2019). Chitin/Chitosan-Active Enzymes Involved in Plant–Microbe Interactions. In Q. Yang, & T. Fukamizo (Eds.), *Targeting chitin-containing organisms* (pp. 253–272). Springer Singapore. https://doi.org/10.1007/978-981-13-7318-3_12.

Gagnaire, D., Saint-Germain, J., & Vincendon, M. (1982). NMR studies of chitin and chitin derivatives. *Die Makromolekulare Chemie, 183*(3), 593–601. https://doi.org/10.1002/macp.1982.021830309

Garádi, Z., Dancsó, A., Piskarev, V., & Béni, S. (2025). From mother's milk to structural insights: 1H–15N NMR analysis of Lewis X antigen-bearing oligosaccharides isolated from human milk. *Carbohydrate Polymers, 347*, Article 122534. https://doi.org/10.1016/j.carbpol.2024.122534

Garádi, Z., Tóth, A., Gáti, T., Dancsó, A., & Béni, S. (2023). Utilizing the 1H-15N NMR methods for the characterization of isomeric human milk oligosaccharides. *International Journal of Molecular Sciences, 24*(3), 2180. https://www.mdpi.com/1422-0067/24/3/2180.

Germer, A., Mügge, C., Peter, M. G., Rottmann, A., & Kleinpeter, E. (2003). Solution- and Bound-State Conformational Study of N,N′,N″-Triacetyl Chitotriose and Other Analogous Potential Inhibitors of Hevamine: Application of trNOESY and STD NMR Spectroscopy. *Chemistry – A European Journal, 9*(9), 1964–1973. https://doi.org/10.1002/chem.200204231

Green, A. R., Li, K., Lockard, B., Young, R. P., Mueller, L. J., & Larive, C. K. (2019). Investigation of the amide proton solvent exchange properties of glycosaminoglycan oligosaccharides. *The Journal of Physical Chemistry B, 123*(22), 4653–4662. https://doi.org/10.1021/acs.jpcb.9b01794

Hu, X., Carmichael, I., & Serianni, A. S. (2010). N-acetyl side-chains in saccharides: NMR J-coupling equations sensitive to CH−NH and NH−CO bond conformations in 2-

Acetamido-2-deoxy-aldohexopyranosyl rings. *The Journal of Organic Chemistry, 75* (15), 4899–4910. https://doi.org/10.1021/jo100521g

Hu, X., Zhang, W., Carmichael, I., & Serianni, A. S. (2010). Amide Cis−trans isomerization in aqueous solutions of methyl N-formyl-d-glucosaminides and methyl N-acetyl-d-glucosaminides: Chemical equilibria and exchange kinetics. *Journal of the American Chemical Society, 132*(13), 4641–4652. https://doi.org/10.1021/ja9086787

Itoh, T., & Kimoto, H. (2019). Bacterial chitinase system as a model of chitin biodegradation. In Q. Yang, & T. Fukamizo (Eds.), *Targeting chitin-containing organisms* (pp. 131–151). Springer Singapore. https://doi.org/10.1007/978-981-13-7318-3_7.

Iwahara, J., Jung, Y.-S., & Clore, G. M. (2007). Heteronuclear NMR spectroscopy for lysine NH3 groups in proteins: Unique effect of water exchange on 15N transverse relaxation. *Journal of the American Chemical Society, 129*(10), 2971–2980. https://doi.org/10.1021/ja0683436

Kashyap, P. L., Xiang, X., & Heiden, P. (2015). Chitosan nanoparticle based delivery systems for sustainable agriculture. *International Journal of Biological Macromolecules, 77*, 36–51. https://doi.org/10.1016/j.ijbiomac.2015.02.039

Langeslay, D. J., Beecher, C. N., Naggi, A., Guerrini, M., Torri, G., & Larive, C. K. (2013). Characterizing the microstructure of heparin and heparan sulfate using N-Sulfoglucosamine 1H and 15N NMR chemical shift analysis. *Analytical Chemistry, 85* (2), 1247–1255. https://doi.org/10.1021/ac3032788

Lescop, E., Schanda, P., & Brutscher, B. (2007). A set of BEST triple-resonance experiments for time-optimized protein resonance assignment. *Journal of Magnetic Resonance, 187*(1), 163–169. https://doi.org/10.1016/j.jmr.2007.04.002

Li, K., Green, A. R., Dinges, M. M., & Larive, C. K. (2019). 1H NMR characterization of chitin tetrasaccharide in binary H2O:DMSO solution: Evidence for anomeric end-effect propagation. *International Journal of Biological Macromolecules, 129*, 744–749. https://doi.org/10.1016/j.ijbiomac.2019.02.062

Meredith, R. J., Tetrault, T., Yoon, M.-K., Zhang, W., Carmichael, I., & Serianni, A. S. (2022). N-acetyl side-chain conformation in saccharides: Solution models obtained from MA'AT analysis. *The Journal of Organic Chemistry, 87*(13), 8368–8379. https://doi.org/10.1021/acs.joc.2c00189

Merzendorfer, H. (2006). Insect chitin synthases: A review. *Journal of Comparative Physiology B, 176*(1), 1–15. https://doi.org/10.1007/s00360-005-0005-3

Mobli, M., & Almond, A. (2007). N-acetylated amino sugars: The dependence of NMR 3J (HNH2)-couplings on conformation, dynamics and solvent. *Organic & Biomolecular Chemistry, 5*(14), 2243–2251. https://doi.org/10.1039/B705761J

Mori, S., Abeygunawardana, C., Johnson, M. O., & Vanzijl, P. C. M. (1995). Improved sensitivity of HSQC spectra of exchanging protons at short interscan delays using a new fast HSQC (FHSQC) detection scheme that avoids water saturation. *Journal of Magnetic Resonance, Series B, 108*(1), 94–98. https://doi.org/10.1006/jmrb.1995.1109

Moussian, B. (2019). Chitin: Structure, chemistry and biology. In Q. Yang, & T. Fukamizo (Eds.), *Targeting chitin-containing organisms* (pp. 5–18). Springer Singapore. https://doi.org/10.1007/978-981-13-7318-3_2.

Pacheco-Arjona, J. R., & Ramirez-Prado, J. H. (2014). Large-scale phylogenetic classification of fungal chitin synthases and identification of a putative cell-wall metabolism gene cluster in aspergillus genomes. *PLoS One, 9*(8), Article e104920. https://www.ncbi.nlm.nih.gov/pmc/articles/PMC4141765/pdf/pone.0104920.pdf.

Peumans, W. J., & Van Damme, E. J. M. (1995). The role of lectins in plant defence. *The Histochemical Journal, 27*(4), 253–271. https://doi.org/10.1007/BF00398968

Pomin, V. H. (2013). Advances in glycosaminoglycanomics by 15N-NMR spectroscopy. *Analytical and Bioanalytical Chemistry, 405*, 3035–3048. https://doi.org/10.1007/s00216-013-6803-7.pdf

Pomin, V. H., Sharp, J. S., Li, X., Wang, L., & Prestegard, J. H. (2010). Characterization of glycosaminoglycans by 15N NMR spectroscopy and in vivo isotopic labeling. *Analytical Chemistry, 82*(10), 4078–4088. https://doi.org/10.1021/ac1001383

Reynolds, W. F., Yu, M., Enriquez, R. G., & Leon, I. (1997). Investigation of the advantages and limitations of forward linear prediction for processing 2D data sets. *Magnetic Resonance in Chemistry, 35*(8), 505–519. https://doi.org/10.1002/(SICI)1097-458X(199708)35:8<505::AID-OMR130>3.0.CO;2-K

Schanda, P., Kupče, Ē., & Brutscher, B. (2005). SOFAST-HMQC experiments for recording two-dimensional heteronuclear correlation spectra of proteins within a few seconds. *Journal of Biomolecular NMR, 33*, 199–211. https://doi.org/10.1007/s10858-005-4425-x.pdf

Schanda, P., Van Melckebeke, H., & Brutscher, B. (2006). Speeding up three-dimensional protein NMR experiments to a few minutes. *Journal of the American Chemical Society, 128*(28), 9042–9043. https://doi.org/10.1021/ja062025p

Sugiyama, H., Hisamichi, K., Sakai, K., Usui, T., Ishiyama, J.-I., Kudo, H., Ito, H., & Senda, Y. (2001). The conformational study of chitin and chitosan oligomers in solution. *Bioorganic & Medicinal Chemistry, 9*(2), 211–216. https://doi.org/10.1016/S0968-0896(00)00236-4

Synowiecki, J., & Al-Khateeb, N. A. (2003). Production, properties, and some new applications of chitin and its derivatives. *Critical Reviews in Food Science and Nutrition, 43*(2), 145–171. https://doi.org/10.1080/10408690390826473

Takashima, T., Ohnuma, T., & Fukamizo, T. (2018). NMR analysis of substrate binding to a two-domain chitinase: Comparison between soluble and insoluble chitins. *Carbohydrate Research, 458*, 52–59. https://doi.org/10.1016/j.carres.2018.02.004

Tokuyasu, K., Ono, H., Ohnishi-Kameyama, M., Hayashi, K., & Mori, Y. (1997). Deacetylation of chitin oligosaccharides of dp 2–4 by chitin deacetylase from Colletotrichum lindemuthianum. *Carbohydrate Research, 303*(3), 353–358. https://doi.org/10.1016/S0008-6215(97)00166-3

Tyrikos-Ergas, T., Bordoni, V., Fittolani, G., Chaube, M. A., Grafmüller, A., Seeberger, P. H., & Delbianco, M. (2021). Systematic structural characterization of chitooligosaccharides enabled by automated glycan assembly. Chemistry–A European Journal, 27(7), 2321–2325. https://www.ncbi.nlm.nih.gov/pmc/articles/PMC7898498/pdf/CHEM-27-2321.pdf.

Van Geet, A. L. (1968). Calibration of the methanol and glycol nuclear magnetic resonance thermometers with a static thermistor probe. *Analytical Chemistry, 40*(14), 2227–2229. https://doi.org/10.1021/ac50158a064

Wishart, D. S., Bigam, C. G., Yao, J., Abildgaard, F., Dyson, H. J., Oldfield, E., … Sykes, B. D. (1995). 1H, 13C and 15N chemical shift referencing in biomolecular NMR. *Journal of Biomolecular NMR, 6*(2), 135–140. https://doi.org/10.1007/BF00211777

Xue, Y., & Nestor, G. (2022). Determination of amide cis/trans isomers in N-acetyl-d-glucosamine: Tailored NMR analysis of the N-acetyl group conformation. *ChemBioChem, 23*(17), Article e202200338. https://doi.org/10.1002/cbic.202200338

Yuwen, T., & Skrynnikov, N. R. (2014). CP-HISQC: A better version of HSQC experiment for intrinsically disordered proteins under physiological conditions. *Journal of Biomolecular NMR, 58*, 175–192. https://doi.org/10.1007/s10858-014-9815-5.pdf